Dalton Transactions

Accepted Manuscript

ROYAL SOCIETY OF CHEMISTRY

www.rsc.org/dalton

Journal Name

RSCPublishing

PERSPECTIVE

Synergy between experimental and theoretical methods in the exploration of homogeneous transition metal catalysis

D. Lupp[a], N. J. Christensen[a] and P. Fristrup[a]*

Cite this: DOI: 10.1039/x0xx00000x

Received ooth January 2012,
Accepted ooth January 2012

DOI: 10.1039/x0xx00000x

www.rsc.org/

In this *Perspective*, we will focus on the use of both experimental and theoretical methods in the exploration of reaction mechanisms in homogeneous transition metal catalysis. We briefly introduce the use of Hammett studies and kinetic isotope effects (KIE). Both of these techniques can be complemented by computational chemistry – in particular in cases where interpretation of the experimental results is not straightforward. The good correspondence between experiment and theory is only possible due to recent advances within the applied theoretical framework. We therefore also highlight the innovations made in the last decades with emphasis on dispersion-corrected DFT and solvation models. The current state-of-the-art is highlighted using examples from the literature with particular focus on the synergy between experiment and theory.

Journal Name RSCPublishing

PERSPECTIVE

Introduction

The idea that application of both theoretical and experimental methods could be beneficial is by no means new – it can be traced back to the famous quotation by Paul Dirac in 1929: "*The underlying physical laws necessary for the mathematical treatment of a large part of physics and the whole of chemistry are thus completely known and the difficulty is only that the exact application of these laws leads to equations much too complicated to be soluble."*[1] In the following sentence Dirac goes on to suggest that *"approximate practical methods of applying quantum mechanics should be developed, which can lead to an explanation of the main features of complex atomic systems without too much computation"*. It is still too early to conclude that the goal set forth by Dirac has been reached, but one could argue that state-of-the-art DFT has come very close. This is particularly true for homogenous transition metal catalysis which, due to relatively limited system sizes (often a few hundred atoms), is amenable to full optimization using density functional theory (DFT) within a reasonable time frame. As a consequence mechanistic investigations in this field now often include a theoretical investigation using DFT.

Due to the success of this approach there exist a vast number of examples in the literature. We have therefore limited the primary focus of this perspective to examples, where both experimental and theoretical studies are contained within the same publication, although we will highlight a few additional examples throughout the perspective. Before starting the survey, we will first introduce competition experiments, an experimental technique that allows for fast and accurate determination of relative reactivity between two substrates. We will also briefly introduce the principles of Hammett studies and kinetic isotope effects (KIE) and discuss some relevant developments in density functional theory calculations.

Competition Experiments

Competition experiments are arguably the simplest way to carry out a mechanistic investigation. Rather than measuring absolute rates of the substrates under investigation in separate flasks, in a competition experiment the two substrates undergo reaction in the same flask. Competition experiments are usually easier to carry out since many factors will necessarily be similar for both substrates (catalyst concentration, reaction temperature etc.).

Often, a first order dependence, regardless of the exact nature of the reacting species, as well as identical reaction orders in all other components, can be assumed. In the context of a catalytic reaction with two substrates (A and B) competing for the active catalyst (cat) this gives the following expressions ([] denotes concentration):

$$\frac{d[A]}{dt} = -k_A[cat][A] \quad (1)$$

$$\frac{d[B]}{dt} = -k_B[cat][B] \quad (2)$$

Division gives:

$$\frac{d[A]}{d[B]} = \frac{k_A}{k_B}\frac{[A]}{[B]} \quad (3)$$

The variables are separated and limits are introduced:

$$\int_{[A]_0}^{[A]} \frac{d[A]}{[A]} = \frac{k_A}{k_B}\int_{[B]_0}^{[B]} \frac{d[B]}{[B]} \quad (4)$$

Which upon integration gives:

$$\ln\left(\frac{[A]_0}{[A]}\right) = \frac{k_A}{k_B}\ln\left(\frac{[B]_0}{[B]}\right) \quad (5)$$

This expression yields a straight line with intercept at y=0, thus by plotting $\ln([A]_0/[A])$ vs. $\ln([B]_0/[B])$ at different levels of conversion, the relative reactivity (k_A/k_B) can be obtained as the slope of the line. If a straight line is *not* obtained, the initial assumption does not hold for the system under investigation, or perhaps some of the compounds are unstable at the conditions employed. An analogous expression can be derived from the appearance of products if that is more convenient for the chemistry being studied.

The experimental differences in reactivity are either directly compared to calculated reactivities (obtained from equation 5), or they are converted to differences in energy (in principle $\Delta(\Delta G^{\ddagger})$) to avoid the exponential dependence.

Hammett Studies

The classical studies of linear free energy relationships have gained renewed attention recently due to the availability of modern computational methods capable of assisting in the interpretation of experimental ρ-values. The method was developed by L. P. Hammett and originated from considering the acidity constants for a series of benzoic acids with different groups in the *para*- or *meta*-positions (Scheme 1)[2] and is now generally referred to as a "Hammett study".[3] From the equilibrium constant a σ-value was assigned to each substituent using σ(H)=0 per definition and all other values proportional to the equilibrium constant for that particular substituent (K_{eq}). A positive σ-value indicates that the substituent is electron-withdrawing, whereas electron-donating substituents lead to negative σ-values.

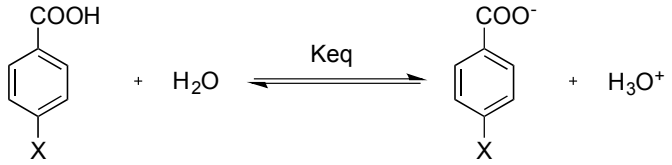

Scheme 1 The acid-base equilibrium of *para*-substituted benzoic acids used by Hammett to define σ-values for a range of different substituents, X.

Hammett was also able to describe the relative *rates* of hydrolysis of the corresponding esters using the same set of σ-values, which established an important connection between equilibrium constants and rate constants. They could be applied to an entire series of related reactions without having to change the σ-values but instead introducing a new parameter (ρ) to account for the different susceptibility of a given reaction to the change in the electronic properties of the substrate (eq. 6).

$$\log\left(\frac{k_X}{k_H}\right) = \sigma_X \rho \quad (6)$$

This new parameter (ρ) is positive when the reaction is accelerated by a decrease in electron-density at the reaction centre and negative when an increase in electron-density leads to rate enhancement. The magnitude of ρ indicates how strongly the rate of the reaction responds to the changes in the electronic properties of the transition state for the rate-determining step, with a typical value of 5-6 for a fully developed ion.[4,5] However, for intermediate values of ρ the use of DFT calculations may aid in the mechanistic interpretation of the results.[6]

The method is especially useful when the reaction is taking place at the benzylic position, allowing for direct conjugation through the π-system of the benzene ring. Since the initial work by Hammett, the method has been developed substantially and a large collection of σ-values is available.[7] In a catalytic reaction the Hammett ρ-value can give information about the overall rate-determining step (if determined using reactions in separate flasks) or the selectivity-determining step (if determined using competition experiments). The selectivity-determining step is the one where the preference for either of the two substrates is determined.

Kinetic Isotope Effects

Determination of kinetic isotope effects (KIE) is one of the most well known methods in physical organic chemistry. It has been reviewed extensively[8] and features prominently in several textbooks.[9] The method is also widely used in organometallic chemistry.[10] Since its introduction in the 1940s by Bigeleisen and Mayer,[11] the methodology has remained popular[12] and there exists a large body of results allowing for direct mechanistic interpretation after determination of the KIE. In particular the relative rate of hydrogen vs. deuterium (k_H/k_D) is often used in determination of kinetic isotope effects. But the phenomenon also occurs for heavier elements such as carbon and chlorine. Here, the small difference in atomic mass between the different isotopes, e.g. $C^{12}/C^{13}/C^{14}$ or Cl^{35}/Cl^{37} makes the KIE determination more experimentally demanding.

In the simple scenario where the reaction proceeds through a single transition state, the KIE can be directly compared to the mechanism of the reaction. If the reaction involves a complete breakage of the bond between carbon and hydrogen/deuterium the KIE is 6.9 at room temperature.[12] This difference arises solely from the difference in zero-point energies (ZPE) and neglects tunnelling (Figure 1). In the more general case, where the bond is merely partially broken, the KIE will be lower than 6.9 due to the existence of a difference in ZPE also at the transition state. The KIE is obviously very temperature-dependent with higher temperatures resulting in smaller observed KIE values in accordance with TS theory relying on an underlying Boltzmann-type behaviour (Figure 1).

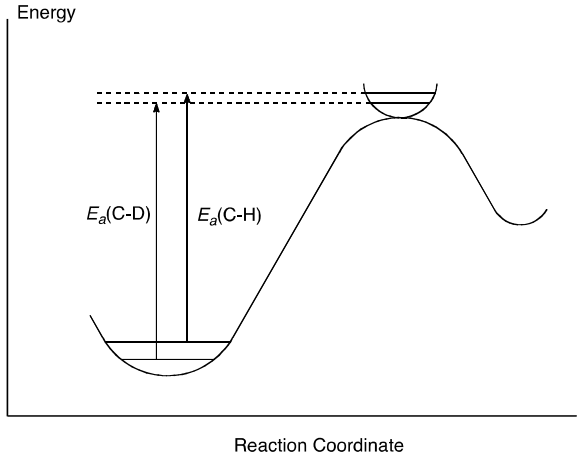

Figure 1 Illustration of how the difference in ZPE caused by the higher mass of deuterium results in a higher barrier towards breakage of the C-H/D bond.

In a catalytic reaction, the situation is more complicated and the measured KIE depends both on the type of measurement (direct competition vs. reaction in separate flasks) and whether or not the step that involves the breakage of the C-H/D bond occurs before or after the rate-determining step. These scenarios have recently been reviewed by Simmons and Hartwig.[13]

DFT Developments

Density functional theory (DFT) is the most widely used quantum mechanical method in theoretical chemistry today.[14] The popularity of DFT is a consequence of its dependence on the electron density, which allows electronic structure calculations with vastly increased computational efficiency relative to wave-function (WF) methods (e.g. coupled cluster theory[15]). For the latter class of methods, realistic system sizes often present an insurmountable computational barrier. In contrast, DFT readily treats large molecules, e.g. transition metal catalysts with entire ligands, as demonstrated below. Importantly, DFT is often associated with a tolerable loss of accuracy compared to WF-methods.[14] Also, DFT is formally exact for any atomic system, provided that the exchange-correlation (E_{XC}) density functional (DF) is known exactly.[16] In

practice, E_{XC} is not exactly known, but a variety of functionals have been, and are being tailored, for particular areas of application. Notwithstanding some interesting developments in certain force field-based methods aimed at describing chemical reactivity (e.g. Q2MM[17] or ReaxFF[18]), DFT remains the only generally applicable method for computations on transition metal-catalysed processes that yields precise results while escaping the need for significant development efforts.

A multitude of methodological and technological advances have contributed substantially to driving DFT improvements and have thus strengthened the foundation for synergistic computational/experimental studies. In particular, improvements in computational efficiency, owing largely to hardware advances,[19] have enabled DFT calculations using realistic system sizes. The introduction of efficient dispersion corrections[20,21] has enabled realistic treatment of long-range, non-covalent interactions, which are essential for large ligands and prediction of stereoselectivity.[22] Also, implicit solvation models[23] have proved important for calculation of accurate energies and reaction barriers. Effective Core Potentials (ECP)[24] are also important in the description of transition metal catalysis, since their use allows implicit treatment of core electrons in heavy elements and partial inclusion of relativistic effects through parameterization.

These and other DFT developments have contributed to the success of several of the case stories (*vide infra*), where the interpretation of the measured KIE was assisted by calculations of plausible reaction steps and/or entire catalytic cycles.

Calculation of Kinetic Isotope Effects and Tunnelling Correction

Kinetic isotope effects are, in most examples herein, calculated within the framework of transition state theory (TST)[25,26]. In TST, the reaction rate is calculated using a Boltzmann type expression. From there, the KIE can simply be obtained using the difference in zero-point energies (ZPEs). At elevated temperatures, the possibility of populating the excited vibrational states must be included, which is possible using the reduced partition function as introduced by Bigeleisen and Mayer[11] and used for similar systems by, for example, the groups of Houk[27] and Singleton.[28]

Since TST is purely classical, quantum mechanical (QM) effects are introduced as corrections to potential energy surface (PES) minima and transition states. The QM corrections to minima are the zero-point vibrational energies, as used in all examples mentioned herein. The QM correction to the transition state is tunnelling.[29] Here, an atom penetrates an energy barrier instead of passing it, leading to increased reaction rates and KIEs compared to TST. Thus, a very large KIE is sometimes considered a diagnostic of tunnelling.[30] Since nuclear tunnelling probability scales inversely with atomic mass, the literature has focused mainly on proton transfers.[31,32] However, recent studies have indicated heavy-atom tunnelling at low temperature (-78 °C) for allylboration of aldehydes[33] and even at room temperature in S_N2 reactions.[34] Thus, nuclear tunnelling may be important at conditions other than at low temperatures and/or for light atoms. However, at the elevated temperatures (>100 °C) in the examples of homogenous transition metal catalysis in this perspective, tunnelling contributions are likely negligible, as the large thermal activation strongly favours barrier passing. Nevertheless, some catalytic studies include a rough estimate for tunnelling effects such as the tunnelling correction due to Wigner.[35,36] In this approach, which applies for small tunnelling effects, and neglects barrier height,[37] the tunnelling corrected rate constant is the TST rate constant multiplied with the factor:

$$\kappa_{\text{Wigner}}(T) = 1 + \frac{1}{24}\left(\frac{h\omega}{k_B T}\right)^2$$

where ω is the TS imaginary frequency, h is Planck's constant, and k_B is Boltzmann's constant. This correction was used in a study of anthracene hydroxylation by De Visser *et al.*[38] and demonstrated mostly negligible effects at ambient conditions for aromatic hydroxylation by Fe(IV)-oxo complexes. However, the KIE associated with hydrogen abstraction increased from 10.5 to 13.2 after applying the Wigner correction.

When substantial tunnelling contributions are expected, reaction rates and KIEs may be calculated e.g. in the framework of canonical variational transition (CVT) state theory[39] using canonically optimized multidimensional tunnelling.[40,41]

DFT Accuracy

An obvious choice, when trying to strengthen the agreement between computational and experimental results, is to carry out calculations at a high level of theory. However, merely adding basis functions does not systematically improve the prediction of experimental KIEs in all cases. This was demonstrated e.g. in the study of gas phase S_N2 reactions,[34] where triple-zeta basis sets (6-311+G(d,p) and aug-cc-pVTZ) in most cases produced larger mean-unsigned errors compared to double-zeta basis sets (6-31+G(d,p), and aug-cc-pVDZ). Also, the choice of density functional requires consideration. For example, the B3LYP[42,43,44,45] functional is popular in general computational chemistry and has been used in several studies on homogeneous transitional metal catalysis. However, B3LYP has certain known deficits. For instance a benchmark of the performance of density functionals for main group thermochemistry, kinetics and non-covalent interactions by Goerigk and Grimme,[46] demonstrated poor performance by B3LYP in the absence of empirical dispersion corrections. Also, B3LYP barrier underestimation by an average of 4.4 kcal/mol was found in a study of main group non-hydrogen transfer reactions by Truhlar *et al.*[47] Poor B3LYP barrier prediction was also found in the Schwartz hydrozirconation reaction,[48] although the agreement with high-level wave-function calculations was improved by including the D3-dispersion correction.

BLYP[43,43,44,44] and B3LYP were found to erroneously predict instability (by ~5.5 kcal/mol) of phosphine binding to Grubbs' ruthenium pre-catalysts for olefin metathesis, whereas the Minnesota functionals, including M06, approximated the experimental binding energy estimate of -3.4

kcal/mol.[49]Another study on Grubbs metathesis catalysis including comparison with NMR, demonstrated an improvement of ~0.5 kcal/mol when using M06 rather than B3LYP for the prediction of conformer stability.[50]

Recently, Steinmetz and Grimme[51] benchmarked 23 density functionals against CCSD(T)/CBS reference data for the computation of Pd- and Ni-catalysed single bond activations in various main group compounds, considering in each case the reactant complex, barrier and reaction energy. They found that the D3 dispersion left barriers unaffected, but had a substantial and positive effect on reaction energies.

In summary, these findings indicate that join-computational studies benefit from prior benchmarking of a variety of DFT functionals and basis sets. Also, the D3 dispersion correction adds little to the computational load and its inclusion generally improves agreement with experiment.

Discussion

Before treating a few examples of synergy in more detail, we want to give an overview over the synergistic effects between experimental and computational mechanistic investigations that have been achieved in the past 10-15 years. We will begin by introducing a number of iron-catalysed processes, which will be followed by studies of rhodium-, iridium-, palladium- and nickel-catalysed reactions.

In 2002, De Visser *et al.* studied the cytochrome P450-catalysed allylic hydroxylation and epoxidation of propene. Through good agreement between experimental and calculated KIE, they were able to determine the nature of the transition state as hydrogen abstraction species.[52] A combined experimental and computational study also helped Li *et al.* in 2009 in determining the spin state of iron in the P450-catalysed oxidation of tertiary amines.[53] In 2012, Kwiecien *et al.* succeeded in determining the exact mechanism for the P450-catalysed oxidative ring opening of the bicyclic amine nortropine.[54] The synergistic approach of experimental and DFT methods was crucial in determining the mechanism of the hydroxylation of anthracene by De Visser *et al.* in 2007,[38] the cross-coupling between aryl chlorides and alkyl magnesium bromides, by Kleimark *et al.* in 2009[55] and the amination of a wide range of allylic and benzylic sp^3 CH-bonds by Liu *et al.* in 2013.[56] For all of these examples, the mechanistic outline was set by experimental evidence while DFT calculations provided more detailed information, such as the precise structure and oxidation state of the metal catalyst.

In the investigation of several rhodium-catalysed reactions, such as the hydrosilylations of ketones by Schneider *et al.* in 2009,[57] the amination of benzylic methylene groups by Nörder *et al.* in 2012[58] and the alkylation of pyrazoles by Algarra *et al.* in 2014[59] DFT calculations helped in the distinction between pathways based on experimental evidence. They were also vital in the rationalization of the experimentally observed unusual regioselectivities in the hydroformylation of a substituted pentene (3,4,4-trimethylpent-1-ene) published by Lazzaronia *et al.* in 2012.[60] For the iridium-catalysed Si-H bond activation of triethyl- and triarylsilanes by Sieh *et al.* in 2013, DFT calculations provided a detailed explanation for the nonlinear Hammett plot by proving the viability of both a nucleophilic and an electrophilic pathway.[61] In the iridium-catalysed C-H activation of benzene by Tenn et al. in 2006[62] and in the hydrogenation of CO_2 by Wang *et al.* in 2012[63] the DFT calculations allowed determination of the exact reaction pathways, which involved rate-determining coordination of benzene and base-assisted heterolysis of H_2, respectively.

The palladium-catalysed amination of aryl chlorides with anillines was investigated by Hoi *et al.* in 2012 by performing a Hammett study that suggested the reductive elimination as rate-determining step. Computational results supported this conclusion and also correctly predicted the order of reactivity for differently substituted substrates.[64] In the Tsuji-Trost alkylation of 2-substituted allylic substrates, Kim *et al.* in 2014, were able to explain the unusual anti-selectivity with a combination of experiments and DFT calculations that favoured the corresponding cationic intermediate.[65] That the application of DFT methods can do more than just explain existing mechanistic proposals and lead to the discovery of new ones was illustrated by Sanchez *et al.* in 2007 for the case of the palladium-catalysed direct arylation of benzoxazoles.[66] A novel ring opening pathway, involving the generation of isocyanophenolate as key intermediate and fast arylation, were supported both by the results obtained in a Hammett study and by DFT calculations.

Comparison of experimental and theoretical KIE values in the Ni-carbene-catalysed dehydrogenation of ammonia borane by Zimmermann *et al.* in 2009[67] and the hydrofluoroarylation of alkynes by Guihaumé *et al.* in 2012,[68] enabled the respective authors to draw conclusions as to the exact nature of the active species and the most likely pathway. The Ni-carbene-catalysed reaction was proposed to proceed through a mono-carbene species with involvement of the carbene in the hydrogen transfer. The hydrofluoroarylation was shown to proceed through a Ni(II)-dialkyl species and not through a Ni(II)-hydride.

To illustrate that the synergistic approach has been applied to the whole range of transition metal-catalysed reactions, we want to highlight a few examples that involve some of the less frequently used transition metals. The first of these is the well-known osmium-catalysed asymmetric dihydroxylation also known as the Sharpless asymmetric dihydroxylation.[69,70] Here, a combined theoretical and experimental KIE studiey by Delmonte *et al.* in 1997 were finally able to provide conclusive evidence in the much debated search for the correct mechanism.[71] Good agreement between the two determined KIE values showed the reaction to proceed via a 3+2 cycloaddition rather than a stepwise mechanism. The next example we want to highlight is the cobalt-catalysed

polymerization of ethane, published by Zeller *et al.* in 2002, for which the experimental KIE matched the calculated one and supported an insertion mechanism for the formation of long chain alkanes.[72] In 2011, Gao *et al.* studied the zinc-catalysed cleavage of a phosphodiester RNA analogue. In their study, an agreement between the experimental and the calculated KIE allowed them to confirm a concerted reaction mechanism over a stepwise one.[73] Finally, DFT calculations, applied to the silver-catalysed insertion of carbenes into alkanes by Flores *et al.* in 2012, were able to correctly reproduce the experimentally observed inability to functionalize methane. This is owed to the fact that the rate-limiting step for methane switches from the carbene formation to the insertion step.[74]

Rhodium-catalysed decarbonylation of aldehydes

The first example we want to discuss in more detail, is the rhodium-catalysed decarbonylation of aromatic aldehydes. This reaction was investigated due to its potential in the valorisation of biomass, as the described transformation reduces the oxygen content of a suitable compound, which is one of the major challenges in biomass utilization.[75]

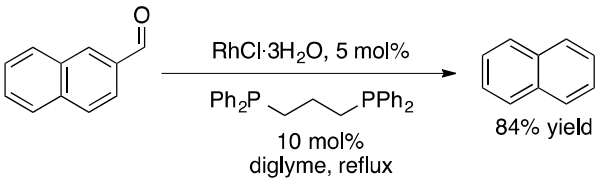

Scheme 2 Rhodium-catalysed decarbonylation of 2-naphtaldehyde.

In 2008, Fristrup *et al*. performed a mechanistic investigation on their previously published reaction shown in Scheme 2.[76,77] The objective of this study was to uncover the mechanism of the decarbonylation reaction through a computational study and confirm the findings by experimental evidence. Based on previously published results, the authors tentatively suggested that the catalytic cycle could consist of oxidation, addition of the aldehyde, migratory extrusion of CO and finally reductive elimination.[78] A KIE of 1.77 for the reaction with benzaldehyde was determined by comparing the reaction rate of benzaldehyde-d_1 with the reaction rate of the undeuterated substrate in a competition experiment. With this method, the full KIE of the selectivity-determining step can be measured even in cases where this step is not the overall rate-determining step.[13]

The computational investigation revealed the rhodium complex carrying an apical hydride and a carbon monoxide to be the energetically most favourable starting point for the reaction. Starting from this complex, the full catalytic cycle was calculated (Scheme 3). The suggested mechanism involves replacement of one of the carbonyl ligands with the aldehyde, as is shown at the top of the scheme. The following oxidative addition of the aldehyde to the metal forms the square pyramidal rhodium hydride shown at the bottom of the figure. The transition state for this transformation is shown in Figure 2. The final steps in the catalytic cycle are migratory extrusion into the acyl C-C bond followed by reductive elimination of benzene.

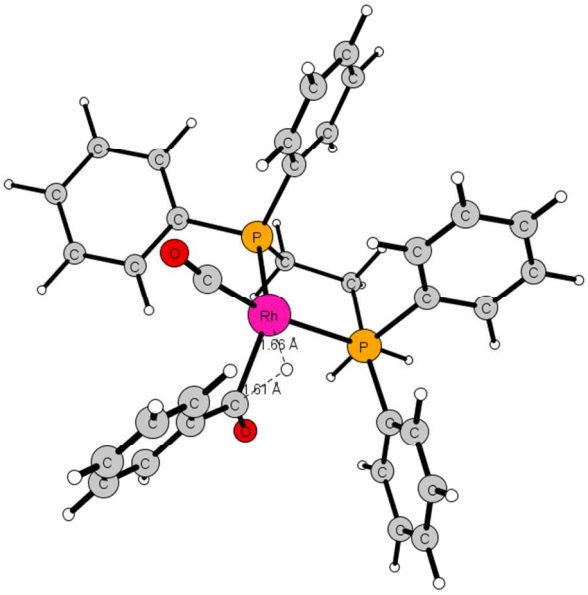

Figure 2 Transition state for the oxidative addition of benzaldehyde to the square-planar rhodium(I) complex. The breaking C-H bond and the forming Rh-H bond are indicated with dashed lines with annotated bond distances.

The Hammett study, performed by the authors, afforded a ρ-value of +0.79, indicating a build-up of negative charge in the rate-determining step, pointing to either the oxidative addition or the migratory extrusion as the rate-determining step.

Journal Name RSCPublishing

PERSPECTIVE

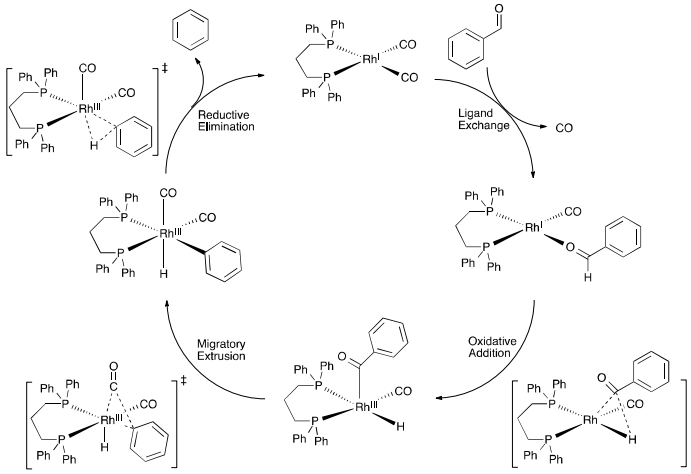

Scheme 3 Final catalytic cycle for the rhodium-catalysed decarbonylation of aldehydes.

A computational estimation of the KIE was carried out, using the initial $[Rh(dppp)CO(PhCHO)]^+$ complex as resting state together with either of the three possible transition states (oxidative addition, migratory extrusion or reductive elimination). The obtained KIE of 1.80, for the calculations assuming the migratory extrusion as rate-determining step, was in very good agreement with the experimental value of 1.77.
Together with the fact that the Hammett ρ-value for the reaction of phenyl acetaldehyde was close to the one for benzaldehyde, this provides strong evidence for the rate-determining nature of the migratory extrusion.
The energetic profile for the decarbonylation is depicted in Figure 3..

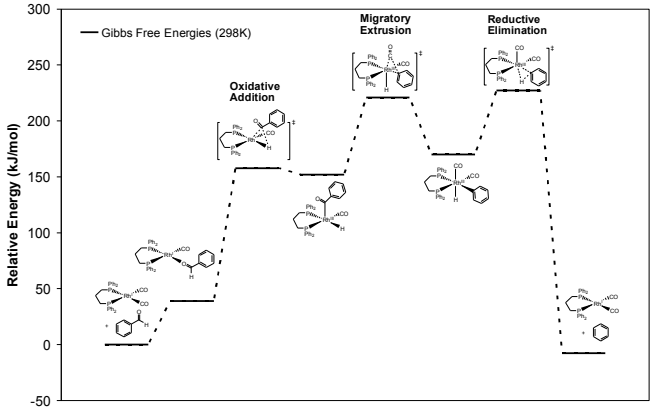

Figure 3 Energy profile for the rhodium-catalysed decarbonylation of benzaldehyde.

IRIDIUM-CATALYSED ALKYLATION OF ALCOHOLS WITH AMINES

The synthesis of carbon-nitrogen bonds lies at the very core of organic chemistry. Their synthesis does, however, often generate stoichiometric amounts of waste due to the use of coupling reagents. A more sustainable and atom-economical transition metal-catalysed approach is therefore desirable. One of the successful methodologies described in recent years is the iridium-catalysed direct coupling of alcohols with amines. The example that we want to discuss here is depicted in Scheme 4.[79] The mechanism of this particular reaction was studied by Fristrup *et al.* in 2012 through a Hammett study for each of the two reactants, determination of kinetic isotope effects and computational modelling of the reaction pathway employing DFT in combination with the B3LYP or the M06 functional.[80]

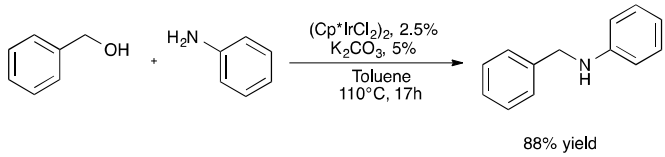

Scheme 4 Iridium-catalysed amination of benzyl alcohol which serves as the model system upon which the mechanistic study is based.

The first Hammett study, performed on a series of *para*-substituted benzyl alcohols, afforded a ρ-value of -0.92, indicating an accumulation of positive charge on the benzylic position during the course of the reaction. The second Hammett study, using *para*-substituted anilines, likewise afforded a negative ρ-value of -1.92. A KIE of 2.48 was found in the competition experiment between α-deuterated benzylalcohol und undeuterated benzylalcohol. These results indicate a rate-determining cleavage of the benzylic C-H bond.
From this finding, the authors concluded the imine formation to be selectivity determining. An imine that was added in a crossover-competition experiment was not reduced under the reaction conditions, which indicated formation and consumption of the imine in the coordination sphere of the iridium catalyst. The monohydridic nature of the active catalyst was determined by the absence of isotope scrambling in an added α-deuterated alcohol.[81] On the basis of these experimental findings, a thorough computational investigation was performed using DFT with either the B3LYP or the M06 functional. The calculation of ΔG for the dissociation of the dimeric starting iridium complex to the monomeric species, using B3LYP, showed the dissociation to be favourable by 22 kJ/mol. The same calculation, using the M06 functional,

predicted the dissociation to be disfavoured by 65 kJ/mol. Overall, it can be assumed that the entropic contribution of dissociation and the presence of competent ligands such as amines and alcohols make the formation of the monomeric species possible. The difference between the results obtained from B3LYP and M06 must arise from the additional stabilization of the dimeric complex due to the contribution of dispersion forces that are partially included in the M06 functional and neglected in the B3LYP functional.

A catalytic cycle was then constructed based on four elementary steps: alcohol oxidation, hemiaminal formation, imine formation (elimination of water), and reduction of the imine (Scheme 5).

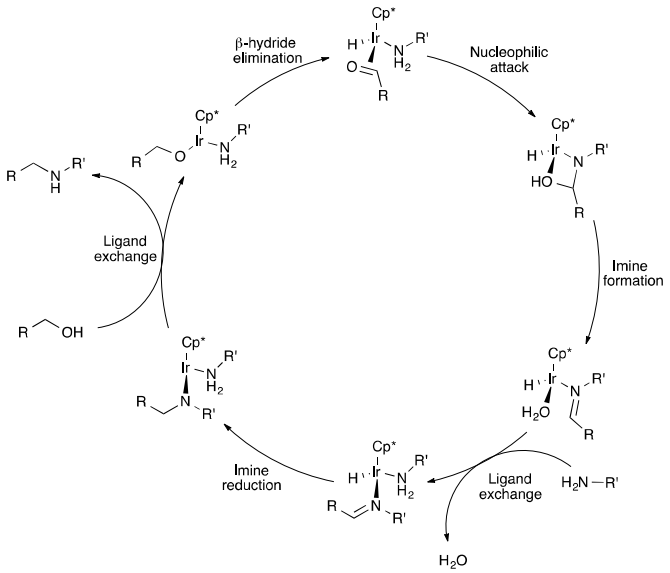

Scheme 5 Full catalytic cycle for the iridium-catalysed amination.

In line with the negative ρ-value obtained in the first Hammett study, the transition state for the β-hydride elimination (Figure 4) shows a significant increase in positive charge on the benzylic carbon atom (ESP charges). Several scenarios for the following hemiaminal formation can be imagined, including nucleophilic attack from differently stabilized internal or external amines. The product of these transformations is an iridium complex that coordinates the hemiaminal and spontaneously forms the corresponding imine-iridium complex. This complex is then reduced by the iridium hydride to afford the final product. The transition state for the reduction is the highest lying point on the potential energy surface and is shown in Figure 4. The KIE and the results from the Hammett studies do not support the reductive elimination as the selectivity-determining step and it can therefore be assumed that the β-hydride elimination assumes that role even though later parts of the catalytic cycle are energetically more demanding. The experimentally determined KIE of 2.48 was matched well by the calculated KIE of 2.70, which is derived from the frequencies for the selectivity-determining step, the β-hydride elimination.

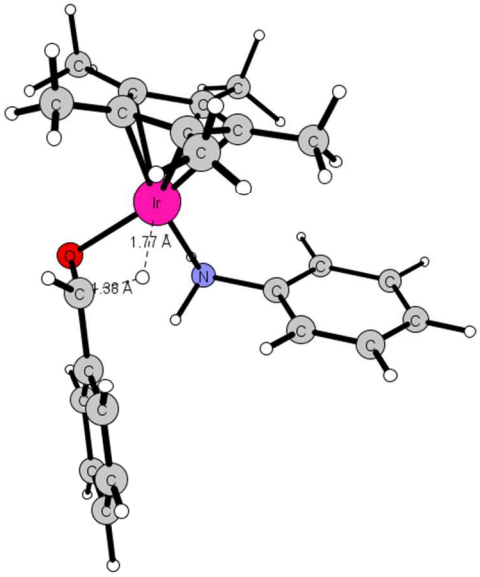

Figure 4 Transition state for the β-hydride elimination in the iridium-catalysed amination of benzaldehyde.

Palladium-catalysed Allylic C-H Alkylation

In 2012, an investigation of the palladium-catalysed allylic C-H alkylation, a reaction that was discovered by White *et al.* in 2008,[82,83] was published by Engelin *et al.* (Scheme 6).[84]

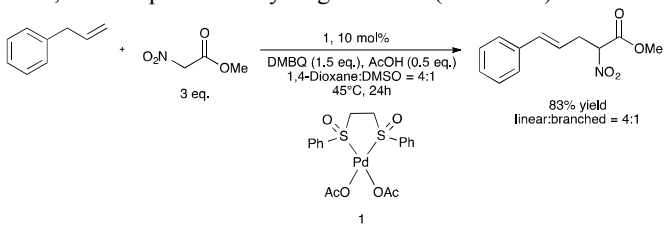

Scheme 6 Palladium-catalysed allylic alkylation by way of C-H activation.

The reaction is an example of a transition metal-catalysed C-H activation, a field that has received an increasing amount of attention in recent years due to its potential as versatile and atom-economic transformation in organic synthesis.[85,86] An experimental study revealed a positive Hammett ρ-value of 0.37, indicating an accumulation of negative charge in the rate determining transition state, suggesting a pathway that involves the abstraction of an allylic proton.

The KIE for the reaction of allylbenzene, fully deuterated in the benzylic position with nitromethane, was measured to be 5.5. Conducting the KIE experiment in two separate flasks, instead of as a direct competition, afforded a significantly lower KIE value of 2.6. This second KIE relates to the whole catalytic cycle, while the previously determined value of 5.5 corresponds to the difference in reactivity in the single step in which the C-H bond is broken.[87] The lower KIE for the overall cycle

indicates the existence of another step that has influence on the rate of the reaction. Isotope scrambling was not observed, which points to the irreversibility of the hydrogen/deuterium transfer reaction. Overall, the experimental results point to a C-H activation in which an irreversible proton abstraction is rate determining.

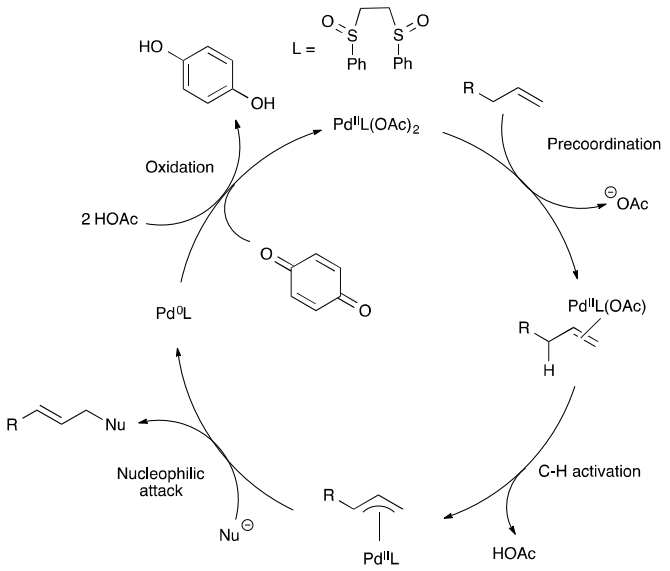

Scheme 7 Proposed catalytic cycle for the palladium-catalysed allylic C-H alkylation.

The authors then performed a computational study of the reaction mechanism utilizing B3LYP-D3, following the general mechanism shown in Scheme 7, which is derived from the mechanism suggested for the classical Tsuji-Trost allylic alkylation.[88] The main question to be answered in this investigation was the nature of the transition state for the hydrogen abstraction, which in the experimental part had been shown to play an important part in the determination of the reaction rate. Fristrup *et al.*[84] suggest five different scenarios for the hydrogen abstraction: two scenarios in which an external acetate, two in which an internal acetate and one in which the sulfoxide ligand participates in the deprotonation, shown in Scheme 8.

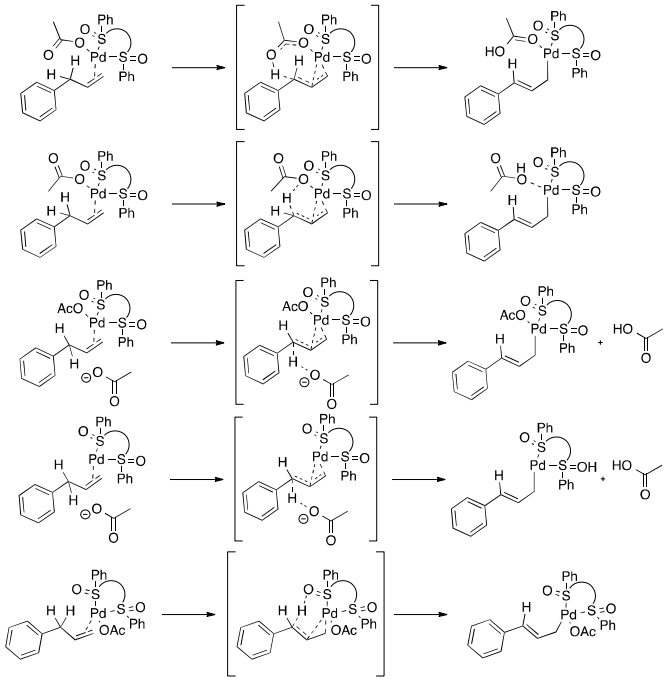

Scheme 8 The five different hydrogen abstraction scenarios studied by Engelin *et al.*: two with deprotonation by internal acetates, two with deprotonation by external acetates and one with deprotonation by the sulfoxide ligand.

The kinetic isotope effects for these five proposals were calculated and showed the reaction to proceed via deprotonation by an internal acetate (*i.e.* an acetate coordinated to palladium) as the computational KIE value for this mechanism of 5.5 exactly matched the experimental value. The structure of the transition state for this deprotonation is shown in Figure 5. The calculated preference of 8:1 for the linear product over the branched product was reasonably well matched by the experimental ratio of 4:1.

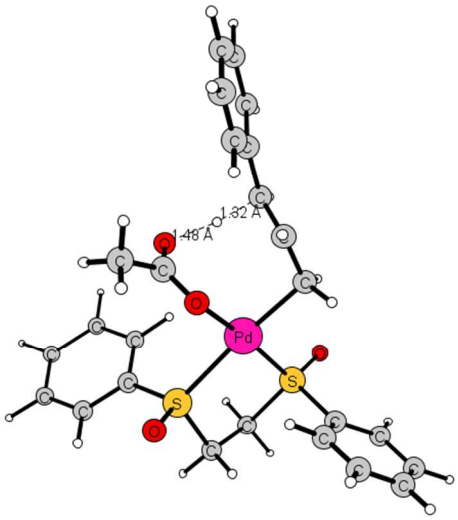

Figure 5 Transition state for the internal acetate abstraction.

The full energy diagram for the final mechanistic proposal is shown in Figure 6.[89]

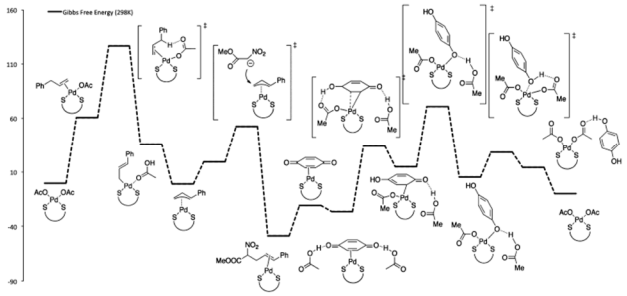

Figure 6 Energy diagram for the final mechanistic proposal in kJ/mol.

The experimental and computational results, in particular the obtained KIE values, match very well and grant credibility to the proposed mechanism illustrating the advantages of the combined approach.

Ruthenium-catalysed Amidation of Alcohols

The next example, we want to highlight, is concerned with the oxidative amidation of benzylic alcohols. This reaction has significant synthetic potential, as amide bonds are one of the most abundant and most important classes of chemical bonds in nature as well as the chemical industry. It is therefore of considerable interest to understand the mechanism of this transformation to not only improve the selectivity and the yield, but also the substrate scope, catalyst loading and catalyst lifetime.

In 2012, Makarov *et al.* studied the mechanism of the reaction shown in Scheme 9,[90] which, as the quantitative isolated yield suggests, was a very clean and effective reaction and therefore ideal for a mechanistic investigation. The reaction was first published by the same group in 2008.[91]

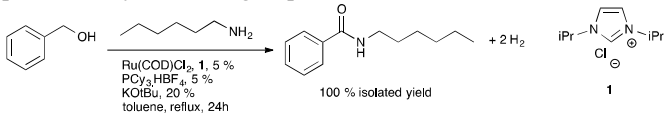

Scheme 9 Ruthenium-catalysed amidation of benzylic alcohol.

A Hammett study was carried out using a series of *para*-substituted benzyl alcohols resulting in ρ-value of -0.15, indicating a small build-up of positive charge at the benzylic position during the rate-limiting step. The small absolute value indicates the likely influence of several steps on the reaction rate. The reaction proved to be first order in ruthenium catalyst, indicating a mono-metal species as active catalyst.

Experiments with alcohols deuterated in the α-position showed rapid scrambling of deuterium with the hydrogens on OH and NH_2, even before the reaction itself had begun, suggesting a reversible β-hydride elimination, the involvement of a dihydride species as intermediate and a migratory insertion step to form dihydrogen. Experiments performed with the diiodide complex instead of the dichloride showed similar initial rates, indicating the absence of halides in the catalytically active species. The KIE for the reaction with the commercially available, fully deuterated 1-butanol was 2.29, suggesting the C-H bond breaking, for example a β-hydride elimination, to have influence on the reaction rate.

NMR studies revealed the presence of ruthenium hydride complexes as well as complexes with and without phosphine. They furthermore showed rapid release of *p*-cymene from ruthenium indicating that the active catalyst most likely does not include *p*-cymene.

To fully elucidate the mechanism of the reaction, a computational study using the M06 functional was undertaken. Most of the overall mechanism, such as the involvement of a β-hydride elimination, a migratory insertion and some details on the structure of the active catalyst, had been determined experimentally. Therefore, the main challenge to be solved by this computational study was to confirm the mechanistic proposal and clarify the fine details such as the distinction between the two pathways in which either the hydride (pathway a) or the amine (pathway b) are located trans to the alkoxide. The full catalytic cycle is shown in Scheme 10.

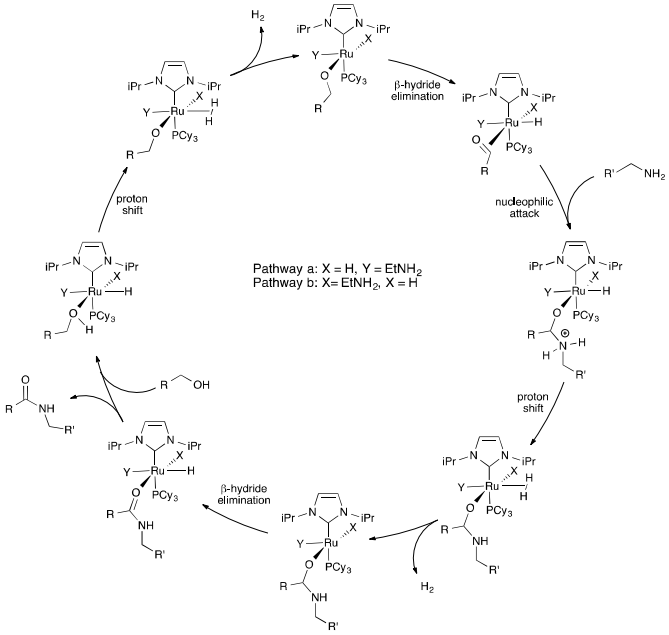

Scheme 10 Proposed catalytic cycles for the ruthenium-catalysed amidation of alcohols. (PCy_3=tricyclohexylphosphine)

The previously mentioned isotope scrambling is endothermic for pathway a and exothermic for pathway b, making pathway b the more likely scenario. Another piece of computational evidence supporting pathway b is the fact that the rate calculated from the energetic span of the whole catalytic cycle is close to the experimentally observed one, while the calculated rate for pathway a is off by a factor of 10^6. The calculations of turnover frequency (TOF) were carried out

using the scheme proposed by Shaik and Kozuch.[92] The calculated KIE for the reaction with benzylamine of 3.78 does not fit well with the experimentally determined value of 2.29. The authors explain this discrepancy with the fact that different amines were used in the experimental and computational parts and propose that the α substituent on the amine has significant influence on the observed KIE. Furthermore, KIE for the related ruthenium-catalysed hydrogenation vary significantly.[93,94]

Overall, the experimental and theoretical results do not match perfectly, but the experimental evidence is still able to sufficiently validate the computational results. This study provides insight into the mechanism of the ruthenium-catalysed oxidative amidation of alcohols that may, as the authors suggest, be used to perform *in-silico* ligand studies in the future.

Iridium-catalysed intramolecular hydroamination

The next example for the synergy between experimental and computational mechanistic investigations, is the iridium-catalysed intramolecular hydroamination published by Hesp *et al.* in 2010.[95] The reaction is fully atom economic and hence in agreement with the general trends and goals of sustainable chemistry.

The optimized reaction conditions, shown in Scheme 11, included the use of an impressively small catalytic amount of the cyclooctadiene iridium chloride dimer in slightly superheated 1,4-dioxane to afford the desired product in 88% isolated yield.

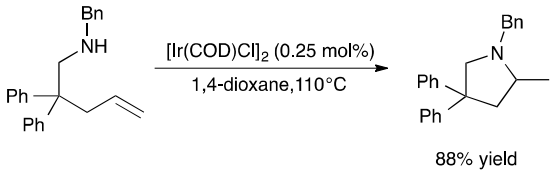

Scheme 11 Reaction conditions for the iridium-catalysed intramolecular hydroamination.

In order to examine the mechanism of this iridium-catalysed hydroamination an experimental as well as computational study were undertaken. Experiments performed, to test the kinetic order of the different constituents of the reaction, showed the reaction to be first order in the catalyst, pointing to a monomeric active catalytic species, and inverse order in substrate, which points to either substrate or product inhibition.

A Hammett study, utilizing a series of *para*-substituted anillines, afforded a ρ-value of -2.4, indicating an accumulation of positive charge in the transition state of the rate-determining step. A kinetic isotope effect study comparing the reaction rates of N-deuterated and undeuterated substrate afforded a KIE of 3.4. This finding suggests the cleavage of the N-H bond to occur in the rate-limiting step, for the details of which, one can envision several different possibilities. A study of the activation parameters for the reaction afforded a reaction enthalpy ΔH* of 20.9 kcal/mol, an activation energy (Ea) of 21.6 kcal/mol and a large negative reaction entropy ΔS*, which points to a highly ordered transition state. Conductivity measurements suggested the absence of chloride in solution during the reaction, indicating coordination of the chloride to the metal throughout the reaction. On the basis of previously suggested mechanisms for similar reactions in the literature, the authors performed a computational study of the C=C bond activation mechanism and the N-H bond activation mechanism shown on the left and the right side of Scheme 12, respectively.

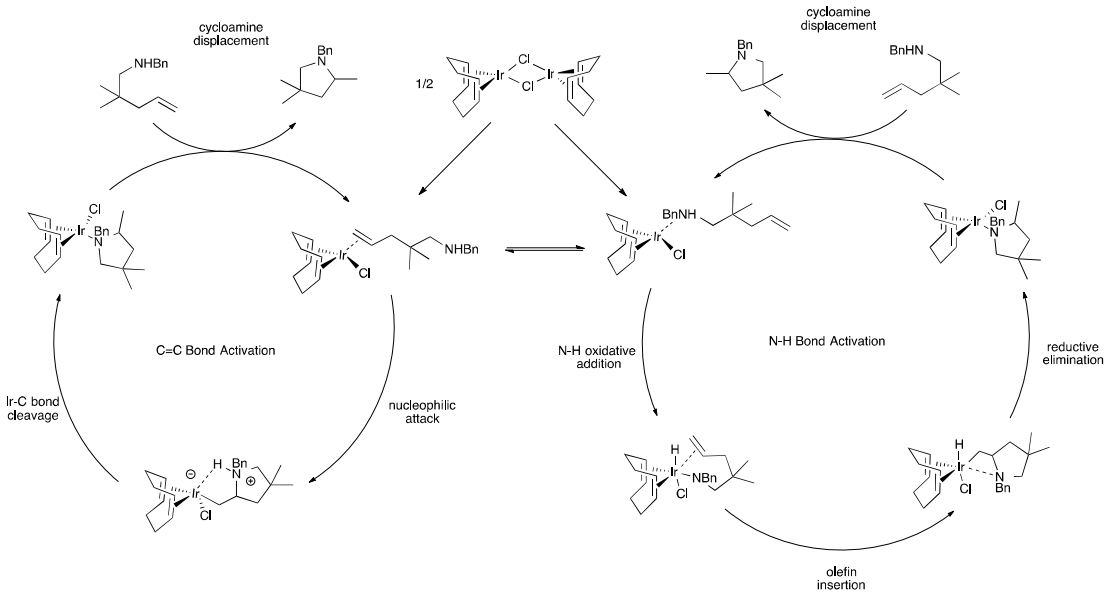

Journal Name RSCPublishing

PERSPECTIVE

Scheme 12 Representation of the two initially suggested mechanisms, C=C bond activation and N-H bond activation.

The first suggested pathway, the N-H bond activation route, starts with the oxidative addition of iridium into the N-H bond. It is followed by insertion of iridium into the olefin, reductive elimination of the alkene and displacement of the cycloamine, which is the final product of the reaction, by another molecule of the starting material. The oxidative addition into the N-H bond has a large activation barrier of 38.2 kcal/mol and is strongly exergonic (ΔG=25.7 kcal/mol). And even though the rest of the mechanism is energetically feasible, the large energy barrier for the first step of this pathway makes it an unlikely candidate.

The second proposed reaction pathway is the C=C bond activation mechanism, in which coordination of the alkene to iridium is followed by nucleophilic attack of the nitrogen on the δ-carbon to form the five-membered ring. Overall protonolysis of the Ir-C bond then liberates the product, which is replaced by another molecule of substrate. This pathway fits with the experimental findings of facile ring-formation, reductive elimination that involves breakage of the Ir-H as rate determining step and the accumulation of positive charge in the rate determining transition state. Furthermore, the calculated total energy barrier of 24.6 kcal/mol fits well with the experimentally determined value of 21.6 kcal/mol. The final proposed catalytic cycle, including some of the elucidated details, is shown in Scheme 13.

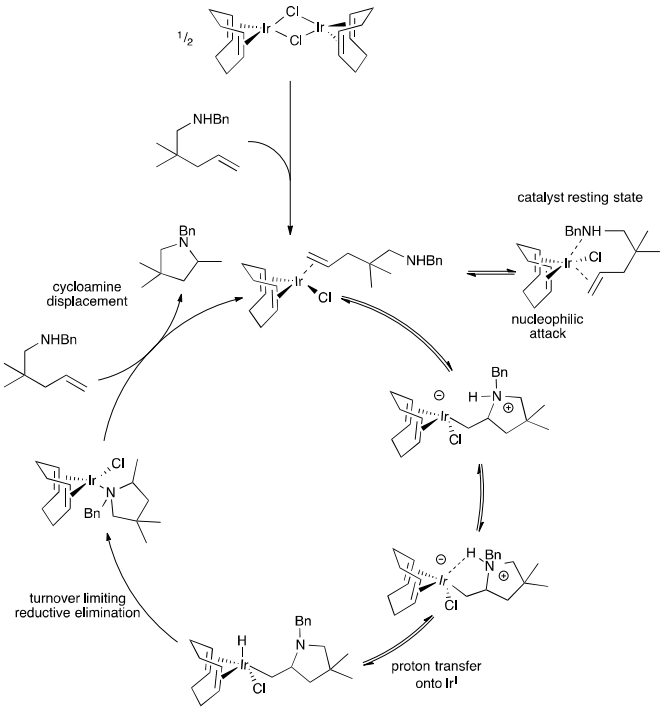

Scheme 13 Final mechanistic proposal for the iridium-catalysed intramolecular hydroamination.

The structure of the transition state for rate-determining reductive elimination is shown in Figure 7.

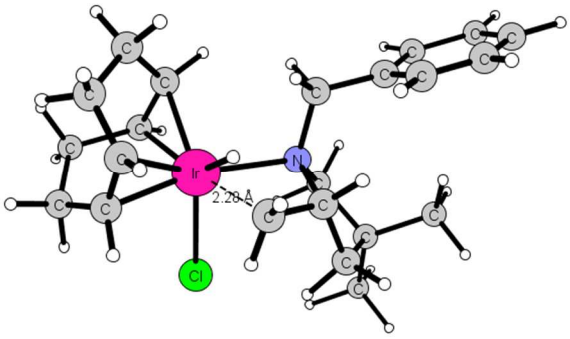

Figure 7 Transition state for the reductive elimination of the cyclic amine. The Ir-C distance of 2.28 Å is indicated in the figure.

Conclusions and Outlook

In this perspective, we have briefly highlighted the developments within computational chemistry over the last decade or so that have enabled near-quantitative description of transition metal-catalysed reactions. We have also introduced some of the most popular experimental approaches, namely determination of kinetic isotope effects and Hammett substituent effects, both of which can often be determined using competition experiments. The level of accuracy that can be expected is highlighted through a series of case studies performed over the last five years that includes catalysis performed by rhodium, iridium, palladium, and ruthenium. The combined use of experimental and theoretical methods have in all cases led to additional insights that were not possible using either of the two separately. The inclusion of experimental results can also be used to benchmark the theoretical methods and provide guidelines for where the theoretical framework should be further developed. It is obvious that the rapid increase in computational resources constantly pushes the boundaries for what chemical challenges can be solved using computational chemistry. We are slowly approaching a time where proficient catalysts can be predicted entirely *in silico*. But, until we reach this goal, the complementary experimental investigations will remain an indispensable tool for the chemical community.

Acknowledgements

Funding from the Danish Council for Independent Research grant no. 11-105487 is gratefully acknowledged. PF would like to express his sincere gratitude to his former graduate supervisors (Prof. David Tanner, Prof. Per-Ola Norrby), post-doctoral supervisors (Prof. Robert Madsen, Prof. Claus Hviid Christensen, and Prof. William A. Goddard, III) and all of the past and present students who have made these combined studies of transition metal-catalysed transformations possible.

Notes and references

[a] Department of Chemistry, Technical University of Denmark, Kemitorvet, building 207, DK-2800 Kgs. Lyngby, Denmark.

1 P. A. M. Dirac, *Proc. R. Soc. Lond. A*, 1929, **123**, 714.
2 L. P. Hammett, *J. Am. Chem. Soc.*, 1937, ***59***, 96.
3 H. H. Jaffé, *Chem. Rev.*, 1953, ***53***, 191.
4 J. Clayden, N. Greeves, S. Warren and P. Wothers, *Organic Chemistry*, Oxford University Press, Oxford, 2001, 1090.
5 E. V. Anslyn and D. A. Dougherty, *Modern Physical Organic Chemistry*, University Science Books, Sausalito, California, 2006, 449.
6 For a recent example, see: J. Mielby, A. Riisager, P. Fristrup and S. Kegnæs, *Catalysis Today*, 2013, **203**, 211.
7 C. Hansch, A. Leo and R. W. Taft, *Chem. Rev.*, 1991, **91**, 165.
8 F. H. Westheimer, *Chem. Rev.*, 1961, **61**, 265.
9 a) N. Isaacs, *Physical Organic Chemistry*, 2nd edition, Longman, Edinburgh, 1995, 287; b) E. V. Anslyn and D. A. Dougherty, *Modern Physical Organic Chemistry*, University Science Books, Sausalito, California, 2006, 421. c) A. Kohen, H.-H. Limbach, *Isotope Effects in Chemistry and Biology,* Taylor & Francis, Boca Raton, 2006.
10 M. Gómez-Gallego and M. A. Sierra, *Chem. Rev.*, 2011, **111**, 4857**.**
11 J. Bigeleisen and M. G. Mayer, *J. Chem. Phys.,* 1947, **15**, 261.
12 F. H. Westheimer, *Chem. Rev.*, 1961, **61**, 265.
13 E. M. Simmons and J. F. Hartwig, *Angew. Chem. Int. Ed.*, 2012, **51**, 3066.
14 C. J. Cramer and D. G. Truhlar *Phys. Chem. Chem. Phys.*, 2009, **11**, 10757.
15 R. J. Bartlett and M. Musiał, *Rev. Mod. Phys.*, 2007, **79**, 291.
16 W. Kohn, *Rev. Mod. Phys.*, 1999, **71**, 1253.
17 P.-O. Norrby, *J. Mol. Struct. (Theochem.)*, 2000, **506**, 9.
18 A. C. T. Van Duin, S. Dasgupta, F. Lorant and W. A. Goddard, III, *J. Phys. Chem. A,* 2001, **105**, 9396.
19 Mack, C. A. *IEEE Trans. Semiconduct. Manufact.,* 2011, **24***,* 202.
20 S. Grimme, *Comput. Mol. Sci.*, 2011, **1**, 211.
21 S. Grimme, J. Antony, S. Ehrlich and H. Krieg, *J. Chem. Phys.*, 2010, **132,** 154104.
22 A. Armstrong, R. A. Boto, P. Dingwall, J. Contreras-Garcia, M. J. Harvey, N. J. Mason and H. S. Rzepa, *Chem. Sci.*, 2014. DOI:10.1039/c3sc53416b
23 C. J. Cramer and D. G. Truhlar, *Chem. Rev.*, 1999, **99**, 2161.
24 T. V. Russo and P. J. Hay, *J. Phys. Chem.*, 1995, **99**, 17085.
25 M. G. Evans and M. Polanyi, *Trans. Faraday Soc.*, 1935, **31**, 875.
26 H. Eyring, *J. Chem. Phys.*, 1935, **3**, 107.
27 K. N. Houk, S. M. Gustafson and K. A. Black, *J. Am. Chem. Soc.*, 1992, **114**, 8565.
28 D. A. Singleton and Z. J. Wang, *Am. Chem. Soc.*, 2005, **127**, 6679.
29 D. Ley, D. Gerbig and P. R. Schreiner, *Org. Biomol. Chem.*, 2012, **10**, 3781.
30 W. J. Albery and M. M. Kreevoy, *Advances in Physical Organic Chemistry*, 1978, **16**, 87.
31 D. G. Truhlar, *J. Phys. Org. Chem.*, 2010, **23**, 660.
32 H.-H. Limbach, J. Miguel Lopez and A. Kohen, *Philos. Trans. R. Soc. B Biol. Sci.*, 2006, **361**, 1399.
33 M. J. Vetticatt and D. A. Singleton, *Org. Lett.*, 2012, **14**, 2370.
34 W.-C. Tsai and W.-P. Hu, *Molecules*, 2013, **18,** 4816.
35 E. Z. Wigner, *F. Physic. Chem.*, 1932, **19**, 203.
36 E. Wigner, *Phys. Rev.*, 1932, **40**, 749.
37 D. W. Ewing and M. J. Manka, *Prepr. Pap.-Am. Chem. Soc., Div. Fuel Chem.*, 2004, **49**, 449.
38 S. P. de Visser, K. OH, A.-R. Han and W. Nam, *Inorg. Chem.*, 2007, **46**, 4632.
39 D. G. Truhlar and B. C. Garrett, *Acc. Chem. Res.*, 1980, **13,** 440.
40 T. N. Truong, D. Lu, G. C. Lynch, Y.-P. Liu, V. S. Melissas, J. J. P. Stewart, R. Steckler, B. C. Garrett, A. D. Isaacson, A. Gonzalez-Lafont, S. N. Rai, G. C. Hancock, T. Joseph and D. G. Truhlar, *Comput. Phys. Commun.*, 1993, **75**, 143.
41 A. Fernandez-Ramos and D. G. Truhlar, *J. Chem. Phys.*, 2001, **114**, 1491.
42 A. D. Becke, *J. Chem. Phys.*, 1993, **98**, 5648.
43 C. Lee, W. Yang and R. G. Parr, *Phys. Rev. B*, 1988, **37**, 785.
44 A. D. Becke, *Phys. Rev. A*, 1988, **38**, 3098.
45 P. J. Stephens, F. J. Devlin, C. F. Chabalowski and M. J. Frisch, *J. Phys. Chem.*, 1994, **98**, 11623.
46 L. Goerigk and S. Grimme, *Phys. Chem. Chem. Phys.*, 2011, **13**, 6670.
47 Y. Zhao, N. González-García and D. G. Truhlar, *J. Phys. Chem. A*, 2005, **109**, 2012.
48 Y. Sun and H. Chen, *J. Chem. Theory Comput.*, 2013, **9**, 4735.
49 Y. Zhao and D. G. Truhlar, *Acc. Chem. Res.*, 2008, **41**, 15.
50 D. Benitez, E. Tkatchouk and W. A. Goddard III. *Organometallics*, 2009, **28**, 2643.
51 M. Steinmetz and S. Grimme, *ChemistryOpen*, 2013, **2**, 115.
52 S P. de Visser, F. Ogliaro, P. K. Sharma and S.Shaik, *J. Am. Chem. Soc.*, 2002, **124**, 11809.
53 C. Li, W. Wu, K.-B. Cho and S. Shaik, *Chem. Eur. J.*, 2009, **15**, 8492.
54 R. A. Kwiecien, K. Kosieradzka, J.-Y. Le Questel, J. Lebreton, A. Fournial, E. Gentil, M. Delaforge, P. Paneth and R. J. Robins, *ChemCatChem*, 2012, **4**, 530.
55 J. Kleimark, A Hedström, P.-F. Larsson, C. Johannson and P.-O. Norrby, *ChemCatChem*, 2009, **1**, 152.
56 Y. Liu, X. Guan, E. L.-M. Wong, P. Liu, J.-S. Huang and C.-M. Che, *J. Am. Chem. Soc.*, 2013, **135**, 7194.
57 N. Schneider, M. Finger, C. Haferkemper, S. Bellemin-Laponnaz, P. Hofmann and L. H. Gade, *Chem. Eur. J.*, 2009, **15**, 11515.
58 A. Nörder, S. A. Warren, E. Herdtweck, S. M. Huber and T. Bach, *J. Am. Chem. Soc.*, 2012, **134**, 13524.

59 A. G. Algarra, W. B. Cross, D. L. Davies, Q. Khamker, S. A. Macgregor, C. L. McMullin and K. Singh, *J. Org. Chem.*, 2014, **79**, 1954.
60 R. Lazzaronia, R. Settambolob, G. Alagonac, C. Ghioc, *J. Mol. Catal. A: Chem.*, 2012, **356**, 1.
61 D. Sieh and P. Burger, *J. Am. Chem. Soc.*, 2013, **135**, 3971.
62 W. J. Tenn, III, K. J. H. Young, J. Oxgaard, R. J. Nielsen, W.A. Goddard, III and R. A. Periana, *Organometallics*, 2006, **25**, 5173.
63 W.-H. Wang, J. F. Hull, J. T. Muckerman, E. Fujita and Y. Himeda, *Energy Environ. Sci.*, 2012, **5**, 7923.
64 K. H. Hoi, S. Calimsiz, R. D. J. Froese, A. C. Hopkinson and M. G. Organ, 2012, C*hem. Eur. J.*, 2012, **18**, 145.
65 B.-S. Kim, M. M. Hussain, P.-O. Norrby and P. J. Walsh, *Chem. Sci.*, 2014, **5**, 1241.
66 R. S. Sánchez and F. A. Zhuravlev, *J. Am. Chem. Soc.*, 2007, **129**, 5824.
67 P. M. Zimmerman, A. Paul and C. B. Musgrave, *Inorg. Chem.*, 2009, **48**, 5418.
68 J. Guihaumé, S. Halbert, O. Eisenstein and R. N. Perutz, *Organometallics*, 2012, **31**, 1300.
69 S.G. Hentges, K.B. Sharpless, *J. Am. Chem. Soc.* 1980, **102,** 4263.
70 E.N. Jacobsen, I. Marko , W.S. Mungall, G. Schröder, K.B. Sharpless, *J. Am. Chem. Soc.*,1988, **110**, 1968.
71 A. J. DelMonte, J. Haller, K. N. Houk, K. B. Sharpless, D. A. Singleton, T. Strassner and A. A. Thomas, *J. Am. Chem. Soc.*, 1997, **119**, 9907**.**
72 A. Zeller and T. Strassner, *Organometallics*, 2002, **21**, 4950.
73 H. Gao, Z. Ke, N. J. DeYonker, J. Wang, H. Xu, Z.-W. Mao, D. Lee Phillips and C. Zhao, *J. Am. Chem. Soc.*, 2011, **133**, 2904.
74 J. A. Flores, N. Komine, K. Pal, B. Pinter, M. Pink, C.-H. Chen, K. G. Caulton and D. J. Mindiola, *ACS Catal.*, 2012, **2**, 2066.
75 J. Zakzeski, P. C. A. Bruijnincx, A. L. Jongerius and B. M. Weckhuysen, *Chem. Rev.*, 2010, **110**, 3552.
76 P. Fristrup, M. Kreis, A. Palmelund, P.-O. Norrby and R. Madsen, *J. Am. Chem. Soc.*, 2008, **130**, 5206.
77 M. Kreis, A. Palmelund, L. Bunch and R. Madsen, *Adv. Synth. Catal.*, 2006, **348**, 2148.
78 D. H. Doughty, M. P. Anderson, A. L. Casalnuovo, M. F. McGuiggan, C. C. Tso, H. H. Wang and L. H. Pignolet, *Adv. Chem. Ser.*, 1982, **196**, 65.
79 K.-J. Fujita and R. Yamaguchi, *Synlett*, 2005, **4**, *560.*
80 P. Fristrup, M. Tursky and R. Madsen, *Org. Biomol. Chem.*, 2012, **10**, 2569.
81 O. Pàmies and J.-E. Bäckvall, *Chem. Eur. J.*, 2001, **23**,5052.
82 A. J. Young and M. C. White, *J. Am. Chem. Soc.*, 2008, **130**, 14090.
83 T. Jensen and P. Fristrup, *Chem. Eur. J.*, 2009, **38**, 9632.
84 C. Engelin, T. Jensen, S. Rodriguez-Rodriguez and P. Fristrup, *ACS Catal.*, 2013, **3**, 294-302.
85 R. H. Crabtree, *Chem. Rev.,* 2010, **110**, 575.
86 A. E. Shilov and G. B. Shul'pin, *Chem. Rev.,* 1997, **97**, 2879.
87 E. Simmons and J. F. Hartwig, *Angew. Chem. Int. Ed.*, 2012, **51**, 3066.
88 B. M. Trost, T. Zhang and J. D. Sieber, *Chem. Sci.,* 2010, **1**, 427.
89 F. Nahra, F. F. Liron, F.,G. Prestat, C. Mealli, C., A. Messaoudi, G. Poli, *Chem.Eur. J.* **2009**, *15*, 11078.
90 I. S. Makarov, P. Fristrup and R. Madsen, *Chem. Eur. J.*, 2012, **18**, 15683.
91 L. U. Nordstrøm, H. Vogt, R. Madsen, *J. Am. Chem.Soc.,* 2008, **130**, 17672.
92 a) A. Uhe, S. Kozuch and S. Shaik, *J. Comput. Chem.*, 2011, **32**, 978; b) S. Kozuch and S. Shaik, *J. Phys. Chem. A*, 2008, **112**, 6032; c) S. Kozuch and S. Shaik, *J. Am. Chem. Soc.*, 2006, **128**, 3355.
93 C. A. Sandoval, T. Ohkuma, K. Muniz and R. Noyori, *J. Am. Chem. Soc.*, 2003, **125**, 13490.
94 M. Zimmer-De Iuliis and R. H. Morris, *J. Am. Chem. Soc.*, 2009, **131**, 11263.
95 K. D. Hesp, S. Tobisch and M. Stradiotto, *J. Am. Chem. Soc.*, 2010, **132**, 413.